AIAA JOURNAL
Vol. 38, No. 9, September 2000

Effect of Plate Thickness on Impedance of Perforated Plates with Bias Flow

Xiaodong Jing* and Xiaofeng Sun†
Beijing University of Aeronautics and Astronautics, 100083 Beijing, People's Republic of China

A numerical model is presented of the Rayleigh conductivity of a square-edged orifice in the presence of finite plate thickness and bias flow. Particular attention is paid to the evaluation of the effect of finite plate thickness on its acoustic impedance. In the presence of bias flow, the acoustic impedance of a kind of perforated plate, which is constructed with square-edged orifices in a plate of finite thickness, is calculated from the Rayleigh conductivity on the assumption that the orifices are well separated. The numerical analysis shows that, although the acoustic resistance increases with the increasing bias flow speed on most occasions, it decreases in a certain range of low bias flow speed, and it can even decrease to negative values for certain combinations of Strouhal number and plate thickness. When the bias flow speed is near zero, increasing plate thickness leads to an increase of the acoustic reactance. However, the acoustic reactance decreases as the bias flow speed is increasing. As a result, the effect of plate thickness on the acoustic reactance will disappear at high bias flow speed. Experimental data are also presented. Qualitatively, the experimental and theoretical results are in good agreement.

Nomenclature

C = complex Rayleigh conductivity
c_0 = sound speed
d = spacing between apertures
H = amplitude of perturbation Bernoulli enthalpy, P/ρ_0
h = perturbation Bernoulli enthalpy
i = $\sqrt{-1}$
k = sound wave number, ω/c_0
$\boldsymbol{k}$ = unit vector in the θ direction
M = average bias flow Mach number through orifice
n = normal coordinate of boundary
n_s = normal coordinate of free streamline of bias flow
$\boldsymbol{n}_s$ = unit vector in the normal direction of free streamline of bias flow
P = amplitude of applied sound pressure
p = applied sound pressure
Q = perturbation volume flux through orifice
R = aperture radius
r = radial coordinate
r_p = normalized specific acoustic resistance by ρc
Sr = Strouhal number, $\omega R/U_c$
s = tangential coordinate along free streamline of bias flow
T = plate thickness
t = time
U_c = convected speed of shed vortices
$\boldsymbol{U}_0$ = mean flow velocity
$\boldsymbol{u}$ = perturbation velocity
x_p = normalized acoustic reactance by ρc
x_1 = axial coordinate
z_p = normalized specific acoustic impedance by ρc; $r_p + ix_p$
γ = $\mathrm{Re}(C/2a)$
γ_e = strength of shed vortex sheet at orifice inlet edge
δ = $-\mathrm{Im}(C/2a)$
θ = circumferential coordinate
ρ_0 = air density
σ = open area ratio
ϕ = perturbation velocity potential
ω = angular frequency
ϖ = strength of shed vortices

Received 20 February 1999; revision received 1 October 1999; accepted for publication 2 November 1999.

*Ph.D. Candidate, Department of Jet Propulsion.
†Professor, Department of Jet Propulsion.

I. Introduction

PERFORATED plates are used extensively to suppress noise and acoustically driven vibrations or instabilities. In some circumstances, for example, in the afterburner of a jet engine, there is a steady cooling airflow through the perforated plates. As a general concern, it is very important to know how a perforated plate with bias flow interacts with the incident pressure wave for the design of highly efficient absorbent liners. Previous investigations[1–3] revealed that the presence of steady bias flow leads to changes of the acoustic impedance of a perforated plate, due to the energy conversion caused by sound vortex interaction. These findings provide a basis for designing a kind of liner with controllable impedance. In fact, the early work of Dean and Tester[4] showed that the acoustic impedance of a perforated liner could be controlled by adjusting flow speed through it. Recently, Zhao and Sun[5] demonstrated that desired acoustic impedance of a perforated liner could be achieved by actively controlling both the flow speed and the cavity depth when the frequency of the incident sound wave varies. These works make evident the potential benefits of a perforated liner with bias flow. Sun and Kaji[6,7] also proposed that some instability phenomena in jet engines, such as flutter, could be suppressed actively by applying this kind of perforated liner as casing treatments.

In view of the practical applications, it is a crucial step to develop a reliable model for the acoustic impedance of a perforated liner with bias flow. Howe[1] presented an analytical method to obtain the Rayleigh conductivity of an orifice in a plate of infinitesimal thickness in the presence of bias flow. Howe's model gives good prediction of the experimental results obtained by Hughes and Dowling.[3] However, in most practical situations, a perforated plate has thickness comparable to the orifice radius, and so a problem arises in determining how plate thickness influences the acoustic properties of a perforated plate. Some investigations[8,9] have been carried out on this aspect recently. After studying on the effect of grazing flow over one or two sides of a perforated plate, Howe[8] concluded that increasing plate thickness could make a perforated plate change its property from absorbing to amplifying sound energy. Tan[9] reported that plate thickness has considerable influence on the resonant frequency of a perforated plate with bias flow when it is backed by a cavity. However, in the situation where there is bias flow through a perforated plate, further investigations in both theoretical and experimental respects are needed to clarify the effect of plate thickness on its acoustic impedance.

The main purpose of this paper is to present a model to take the effect of plate thickness into consideration when studying the acoustic properties of a perforated plate with bias flow through it. Previous experimental and theoretical works[1–3,8] show that unsteady vortices

are generated due to the viscous effect when a sound wave is incident on a sharp edge and the shed vortices are subsequently convected away from the sharp edge in the presence of a steady flow. Based on this interaction mechanism, this paper presents a model to study the acoustic properties of a square-edged orifice in a plate of small, but finite thickness with steady flow through it. The steady flow is assumed to separate from the inlet edge of the orifice, and the Kutta condition is applied at the inlet edge to determine the strength of the unsteady shed vortices. To consider the effect of the tube wall of the orifice, the governing equation derived by Howe[1] is solved numerically by the boundary element method. To validate the theoretical results, an experiment is designed in the present investigations, in which the acoustic impedance of a perforated plate with bias flow is measured by the two-microphone method. Qualitatively, the theoretical predictions are in good agreement with the experimental data presented in this paper.

II. Basic Equations

As shown in Fig. 1, an orifice is located in a plate of small, but finite thickness, and there is a low Mach number, high Reynolds number steady flow through the orifice. The flow separates from the inlet edge of the orifice and forms a jet. A cylindrical coordinate system (x_1, θ, r) is introduced. Consider a uniform sinusoidal pressure perturbation in the region $x_1 < 0$:

$$p = P \exp(-i\omega t) \tag{1}$$

This pressure perturbation can be produced by a low-frequency sound wave incident on the plate. The pressure perturbation leads to the unsteady vortices shed from the inlet edge of the orifice, and the shed vortices are convected away along the mean streamline. Because the Mach number of the mean flow is low and the wavelength of the incident sound wave greatly exceeds the orifice radius at low frequency, it is reasonable to consider the flow as incompressible in the vicinity of the orifice. The flowfield is also assumed to be inviscid, and the viscous effect is only taken into consideration by applying the Kutta condition at the inlet edge. Based on the preceding assumption, the governing equations are the incompressible Euler equations. If we introduce the hypothesis that the convection of the unsteady vortex plays dominant role and the perturbation of the mean shear layer is ignored, the linearized Euler equation can be rewritten, according to Howe,[1] as follows:

$$\nabla^2 h = -\nabla \cdot (\boldsymbol{\varpi} \times \boldsymbol{U}_0) \tag{2}$$

where perturbation Bernoulli enthalpy h is defined by the following relation:

$$h = \frac{p}{\rho_0} + \boldsymbol{U}_0 \cdot \boldsymbol{u} = -\frac{\partial \phi}{\partial t} + cc \tag{3}$$

where cc is a constant that takes different values in the two regions of potential flow separated by the free shear layer of the bias flow.

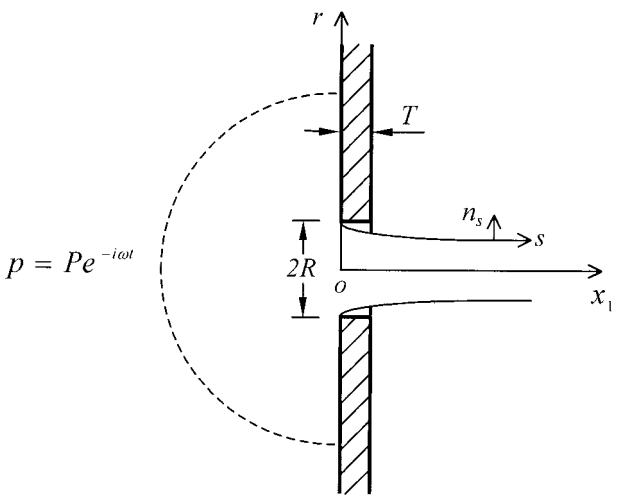

Fig. 1 Orifice in a thick plate with steady bias flow.

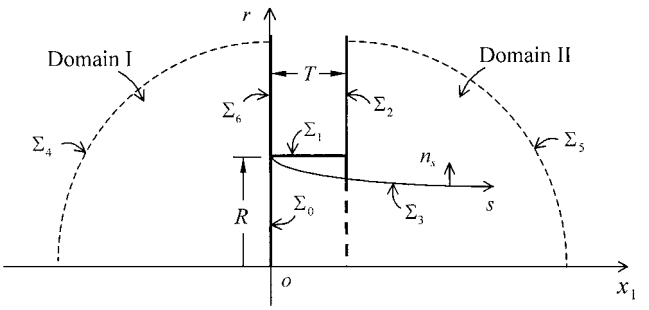

Fig. 2 Arrangement of the integration domains and the integration surfaces.

On the condition of high Reynolds number based on the mean flow speed and orifice radius, the shear layer is very thin. The strength of the unsteady vortices can be written as

$$\boldsymbol{\varpi} = \gamma_e \exp[-i\omega(t - s/U_c)]\delta(n_s)\boldsymbol{k} \tag{4}$$

Substituting Eq. (4) into Eq. (2) and suppressing the time-dependent part, $\exp(-i\omega t)$, we obtain the following axisymmetric Possion equation:

$$\frac{1}{r}\frac{\partial}{\partial r}\left(r\frac{\partial h}{\partial r}\right) + \frac{\partial^2 h}{\partial x_1^2} = -\nabla \cdot \left[\gamma_e U_c \exp\left(\frac{i\omega s}{U_c}\right)\delta(n_s)\boldsymbol{n}_s\right] \tag{5}$$

By the application of the half-space Green function, Eq. (5) can be converted into integral equations. As shown in Fig. 2, the integration space is divided into two domains that are separated by boundary Σ_0. The surfaces in Fig. 2 are explained as follows: Σ_0 is where $x_1 = 0$ and $r < R$, Σ_1 is where $0 \le x_1 \le T$ and $r = R$, Σ_2 is where $x_1 = T$ and $r > R$, Σ_3 is the freestream surface, Σ_4 is where $x_1 < 0$ and $x_1^2 + r^2 \to \infty$, Σ_5 is where $x_1 > 0$ and $x_1^2 + r^2 \to \infty$, and Σ_6 is where $x_1 = 0$ and $r > R$.

To solve Eq. (5), the following boundary conditions are applied:

$$\frac{\partial h}{\partial n} = 0, \qquad \text{on the solid wall}$$

$$h = H, \qquad \frac{\partial h}{\partial n} = 0, \qquad \text{on } \Sigma_4$$

$$h = 0, \qquad \frac{\partial h}{\partial n} = 0, \qquad \text{on } \Sigma_5 \tag{6}$$

The half-space Green G_h function satisfies

$$\nabla^2 G_h = \delta(\boldsymbol{x} - \boldsymbol{y}), \left.\frac{\partial G_h}{\partial y_1}\right|_{y1=0} = 0 \tag{7}$$

In a cylindrical coordinate system, it is expressed as follows:

$$G_h(x_1, \theta, r; y_1, \varphi, \rho) = -\frac{1}{4\pi}\left[\frac{1}{\sqrt{(x_1 - y_1)^2 + r^2 + \rho^2 - 2\rho r\cos(\theta - \varphi)}} + \frac{1}{\sqrt{(x_1 + y_1)^2 + r^2 + \rho^2 - 2\rho r\cos(\theta - \varphi)}}\right] \tag{8}$$

Finally, the expressions of h are obtained. In the domain $x_1 < 0$,

$$h = H - \int_{\Sigma_0} \frac{\partial h}{\partial y_1} G_h \, \mathrm{d}S \tag{9}$$

In the domain $x_1 > 0$,

$$ch = \int_{\Sigma_0} \frac{\partial h}{\partial y_1} G_h \, \mathrm{d}S + \int_{\Sigma_1} h\frac{\partial G_h}{\partial \rho} \, \mathrm{d}S - \int_{\Sigma_2} h\frac{\partial G_h}{\partial y_1} \, \mathrm{d}S - \int \nabla \cdot \left[\gamma_e U_c \exp\left(\frac{i\omega s}{U_c}\right)\delta(n_s)\boldsymbol{n}_s\right] G_h \, \mathrm{d}V \tag{10}$$

where $c = \frac{1}{2}$ on the boundary and $c = 1$ in the domain. After integrating the last integral in Eq. (10) by parts and carrying out the integration of δ function, the volume integral can be converted to surface integral, so that Eq. (10) is simplified as follows:

$$ch = \int_{\Sigma_0} \frac{\partial h}{\partial y_1} G_h \, dS + \int_{\Sigma_1} h \frac{\partial G_h}{\partial \rho} \, dS - \int_{\Sigma_2} h \frac{\partial G_h}{\partial y_1} \, dS - \int_{\Sigma_3} \gamma_e U_c \exp\left(\frac{i\omega s}{U_c}\right) \frac{\partial G_h}{\partial n_s} \, dS \tag{11}$$

In the inlet cross section of the orifice, the perturbation Bernoulli enthalpy and its normal derivative are continuous,

$$\frac{\partial h}{\partial x_1}(x_1 = 0^+, r) = \frac{\partial h}{\partial x_1}(x_1 = 0^-, r)$$
$$h(x_1 = 0^+, r) = h(x_1 = 0^-, r) \tag{12}$$

Equations (9) and (11) are related to each other by the continuous condition (12), and so the following integral equations can be derived:

$$H - 2\int_{\Sigma_0} \frac{\partial h}{\partial y_1} G_h \, dS - \int_{\Sigma_1} h \frac{\partial G_h}{\partial \rho} \, dS + \int_{\Sigma_2} h \frac{\partial G_h}{\partial y_1} \, dS + \int_{\Sigma_3} \gamma_e U_c \exp\left(\frac{isSr}{R}\right) \frac{\partial G_h}{\partial n} \, dS = 0 \qquad (\text{on } \Sigma_0) \tag{13}$$

$$\frac{1}{2}h - \int_{\Sigma_0} \frac{\partial h}{\partial y_1} G_h \, dS - \int_{\Sigma_1} h \frac{\partial G_h}{\partial \rho} \, dS + \int_{\Sigma_2} h \frac{\partial G_h}{\partial y_1} \, dS + \int_{\Sigma_3} \gamma_e U_c \exp\left(\frac{isSr}{R}\right) \frac{\partial G_h}{\partial n} \, dS = 0 \qquad (\text{on } \Sigma_1 \text{ or } \Sigma_2) \tag{14}$$

where $Sr = \omega R / U_c$ is the Strouhal number. The strength of the shedding vortex sheet γ_e is determined by applying the Kutta condition, which requires the normal derivative of the Bernoulli enthalpy to be zero at the inlet edge of the orifice; that is,

$$\frac{\partial h}{\partial x_1}(x_1 = 0, r = R^-) = 0 \tag{15}$$

It is equivalent to requiring the normal velocity to be zero there.

III. Numerical Implementation and Numerical Results

Equations (13–15) are solved numerically by the boundary element method. The variables are normalized as

$$\bar{x}_1 = x_1/R, \qquad \bar{r} = r/R, \qquad \bar{T} = T/R, \qquad \bar{h} = h/\rho_0 \omega^2 R^2$$
$$\bar{\gamma}_e = \gamma_e/\omega R, \qquad \bar{U}_c = U_c/\omega R = 1/Sr$$

By the advantage of the axisymmetry, the surface integrals in Eqs. (13) and (14) can be reduced to the line integrals. The line integrals are evaluated by 10-point Gaussian quadrature. On Σ_0, the unknown variable is $\partial\bar{h}/\partial\bar{x}_1$, and on Σ_1 and Σ_2 the unknown variable is $\bar{h}$. The upper limit on Σ_2 is truncated at $200R$. The number of the control points on Σ_0, Σ_1, and Σ_2 are N_0, N_1, and N_2 and respectively, and the total number of the control points are $N = N_0 + N_1 + N_2$. The last term of both Eqs. (13) and (14) is the contribution of the unsteady vortex sheet, and the only unknown is the vortex sheet strength $\bar{\gamma}_e$ at the leading edge. The geometry of the free streamline is obtained from the interpolation of the experimental data in Ref. 10. The upper length of the streamline is truncated at $100R$. Equations (13) and (14) are discretized into the following linear equations:

$$\sum_{j=1}^{N} a_{ij}\lambda_j - b_i \bar{U}_c \bar{\gamma}_e = H \qquad (1 \le i \le N_0)$$

$$\sum_{j=1}^{N} a_{ij}\lambda_j - \frac{1}{2}\lambda_i - b_i \bar{U}_c \bar{\gamma}_e = 0 \qquad (N_0 + 1 \le i \le N)$$

$$\lambda_i = \begin{cases} \dfrac{\partial \bar{h}}{\partial \bar{x}_1}(x_{1i}, r_i) & (1 \le i \le N_0) \\ \bar{h}(x_{1i}, r_i) & (N_0 + 1 \le i \le N) \end{cases} \tag{16}$$

$P(x_{1i}, r_i)$ are the control points on the integral surfaces. The influence coefficients a_{ij} and b_i are evaluated using the method described in Ref. 11. The Kutta condition (15) is approximately given by

$$\lambda_i = 0 \qquad (i = N_0) \tag{17}$$

The linear equations in Eq. (16) together with Eq. (17) are solved by the Gauss elimination method. Particular care is taken around the geometrical singularity at edges of the orifice by decreasing the distances between the control points near to the edges.

The Rayleigh conductivity C is defined by the relation

$$C = \frac{i\omega\rho_0 Q}{p_+ - p_-} \tag{18}$$

where $p_+ - p_-$ is the applied pressure difference across the orifice and the volume flux Q is given by

$$Q = \frac{1}{i\omega} \int_{\Sigma_0} \frac{\partial h}{\partial x_1} \, dS \tag{19}$$

The Rayleigh conductivity of an orifice in a thin plate is equal to $2R$ when there is no mean flow through it. Thus, C and Q are normalized as

$$\bar{C} = C/2R, \qquad \bar{Q} = Q/\pi\omega R^3$$

Then

$$\bar{C} = \gamma - i\delta = -(i\pi\bar{Q}/2\bar{H}) \tag{20}$$

where γ and δ are the functions of two parameters, the Strouhal number Sr and the nondimensional thickness $\bar{T}$. When $\bar{T} \to 0$ and the shape of the vortex sheet is selected to be cylindrical, the present numerical results of the normalized Rayleigh conductivity are compared with the analytical results of Howe.[1] The consistency is validated by the good agreement between them, as shown in Fig. 3. In Fig. 4, the normalized Rayleigh conductivity is plotted as a function of the Strouhal number for different nondimensional thickness. As shown in Fig. 4b, when $\bar{T} = 2.0$, δ is negative in range of

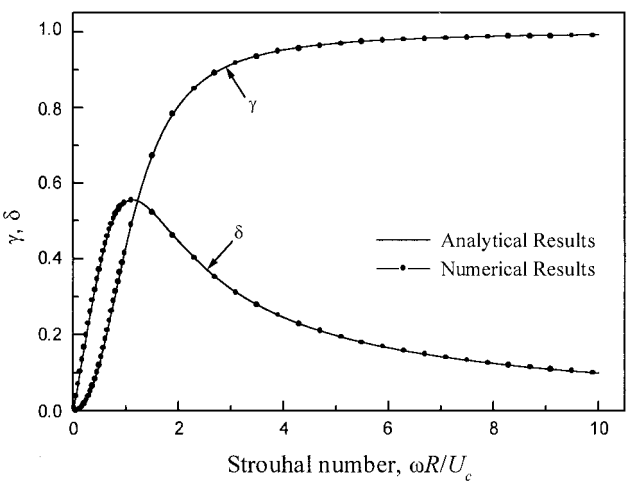

Fig. 3 Comparison between numerical and analytical results of the normalized Rayleigh conductivity.

$1.08 < Sr < 1.48$. Further numerical tests show that, when $\bar{T} > 1.5$, there exists a certain range of Strouhal number where δ is negative. Contrary to this result, the analytical results of Ref. 1 show that δ is always positive in the situation of an infinitely thin plate.

IV. Experiment

The experimental setup is shown in Fig. 5. A two-microphone technique developed by Johnston and Schmidt[12] is employed to measure the impedance of perforated plates with bias flow. The impedance tube is 1 m (39.37 in.) long, and its cross section is a 100×100 mm (3.94 in.) square. The first cutoff frequency of the impedance tube is 1715 Hz. At one end of the impedance tube is the sound source, which consists of four loudspeakers; at the other end is the test perforated plate. Two $\frac{1}{4}$-in. (6.35-mm) microphones are mounted flush with the inner surface of the impedance tube, and the spacing between them is 100 mm (3.94 in.). The distance between the test perforated plate and the nearest microphone is 300 mm (11.32 in.) An anechoic chamber is connected to the impedance tube just behind the test perforated plate, and its cross section is the same as that of the impedance tube. The inner wall of the anechoic chamber is lined with sound absorbing materials. A sound absorbing wedge made of foam is installed inside the anechoic chamber, and there is a cavity beween the wedge and the back wall of the anechoic chamber. The absorption coefficient of the anechoic chamber is over 0.99 above 200 Hz. There are four airflow inlets in the back wall of the chamber, through which steady, but adjustable, airflow enters the anechoic chamber. The volume flux of the airflow is measured by a rotameter. The airflow goes through the test perforated plate and the impedance tube, then flows into the air at the end of the loudspeakers. In the present experiment, an harmonic sound source is used. According to Ref. 12, the acoustic impedance of the test perforated plate can be calculated from the amplitudes of the sound pressures at two locations along the impedance tube and the phase difference between the sound pressures, which are measured by the two microphones. The sound pressure level (SPL) in the impedance tube is kept within the range 90–120 dB. It has been checked that over this range the measured acoustic impedance is independent of the SPL. Four different perforated plates are selected to test their acoustic impedance in the presence of bias flow. For all of the test perforated plates, the orifices are arranged in square arrays. The geometry of a typical perforated plate constructed with square-edged orifices is shown in Fig. 6. The geometrical parameters of the test perforated plates are shown in Table 1.

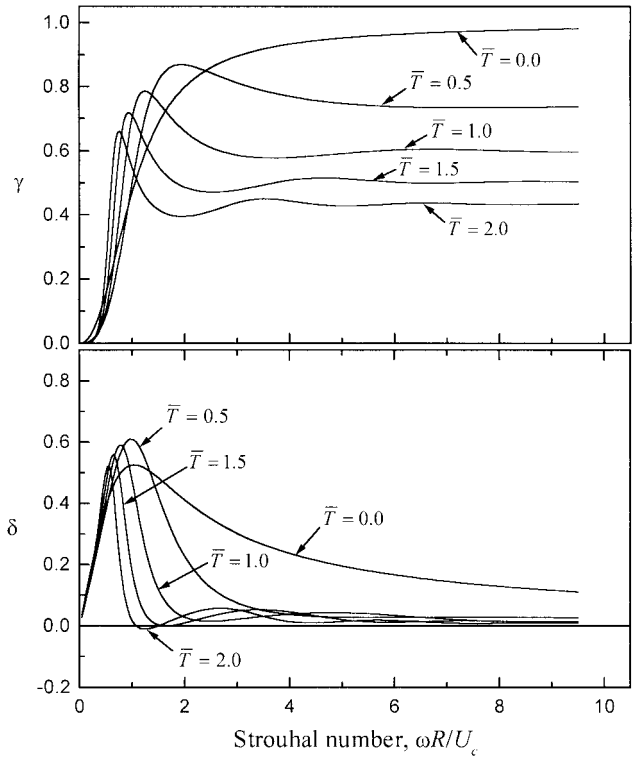

Fig. 4 Normalized Rayleigh conductivity as a function of Strouhal number for different nondimentional plate thickness.

Table 1 Geometrical parameters of the test perforated plates

Number	R, mm (in.)	D, mm (in.)	T, mm (in.)	σ, %
1	1.6 (0.0630)	20 (0.787)	2.0 (0.0787)	1.29
2	2.0 (0.0787)	30 (1.181)	2.0 (0.0787)	1.13
3	2.5 (0.0984)	30 (1.181)	2.0 (0.0787)	1.77
4	2.5 (0.0984)	30 (1.181)	3.0 (0.1181)	1.77

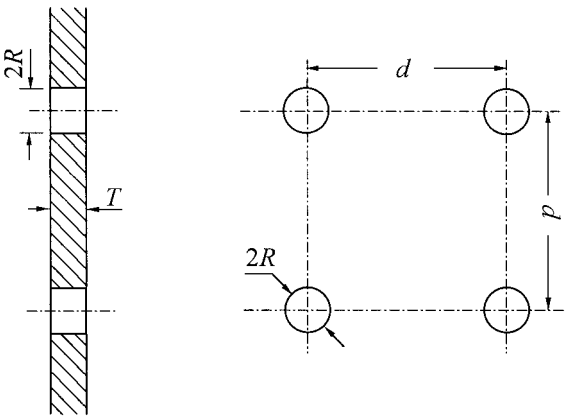

Fig. 6 Perforated plate geometry.

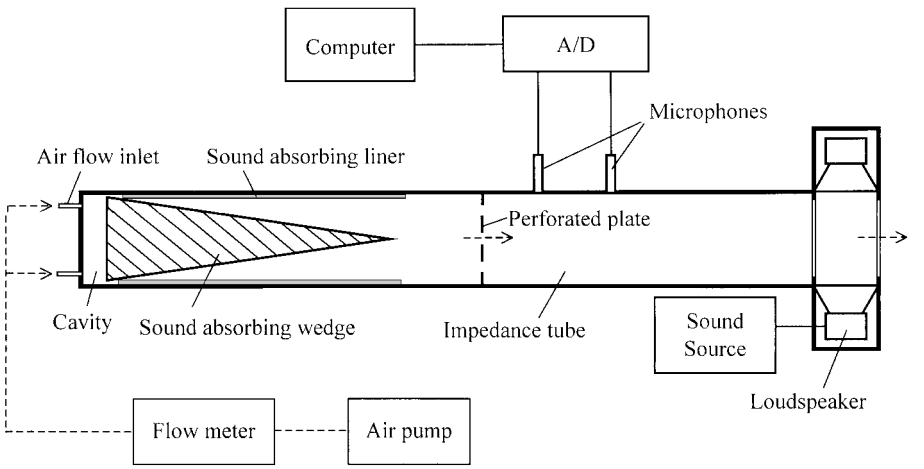

Fig. 5 Schematic of the experimental setup; dashed arrows indicate the path of the airflow.

V. Results and Discussion

Provided that the spacing between the orifices is far larger than the orifice radius, the normalize specific acoustic impedance z_p of a perforated plate is related to the Rayleigh conductivity $C = 2R(\gamma - i\delta)$ as follows:

$$z_p = \frac{p_- - p_+}{\rho_0 c_0 u} = \left(\frac{\pi kR}{2\sigma}\right)\left(\frac{\delta}{\gamma^2 + \delta^2} - i\frac{\gamma}{\gamma^2 + \delta^2}\right) \tag{21}$$

where u is the normal acoustic particle velocity on the surface of the perforated plate. We also try to calculate the normalized specific acoustic impedance of a thick perforated plate with bias flow by an analytical model. The analytical results of Howe[1] are employed to calculate the normalized specific acoustic impedance of a thin perforated plate with bias flow. If the normalized specific acoustic impedance of a thin perforated plate is considered as the end correction z_e, that of the corresponding thick one can be tentatively written as

$$z_p = z_e - ikT/\sigma \tag{22}$$

The last term of Eq. (22) is due to the thickness of the perforated plate. In both the numerical and the analytical calculations, the convected speed of the shed vortices U_c is taken as average bias flow speed through the orifice. The Strouhal number $Sr = \omega R/U_c$ can be rewritten as

$$Sr = kR/M \tag{23}$$

Thus, the acoustic impedance given both by Eqs. (21) and (22) is the function of three nondimensional parameters: the bias flow Mach number M, the Helmholtz number kR, and the nondimensional plate thickness T/R.

In Figs. 7–10, the numerical results of Eq. (21) and the analytical results of Eq. (22) are compared with the experimental data. The normalized specific acoustic resistance r_p and normalized specific acoustic reactance x_p are plotted as the functions of the bias flow Mach number M at given Helmoholtz number kR. The obvious discrepancy between the results of Eq. (22) and the experiment, especially for the normalized specific acoustic reactance, shows that the normalized specific acoustic impedance of a thick perforated plate with bias flow is more complicated than a simple combination of the thickness term $-ikT/\sigma$ with the end correction. The complexity arises from the separation of the mean stream from the inlet edge of an orifice. The present numerical model takes this factor into consideration, and so the numerical results qualitatively give a good prediction of the experimental data.

The results of Figs. 7–10 show that, in the presence of bias flow, plate thickness influences the normalized specific acoustic reactance in a completely different way from the situation without bias

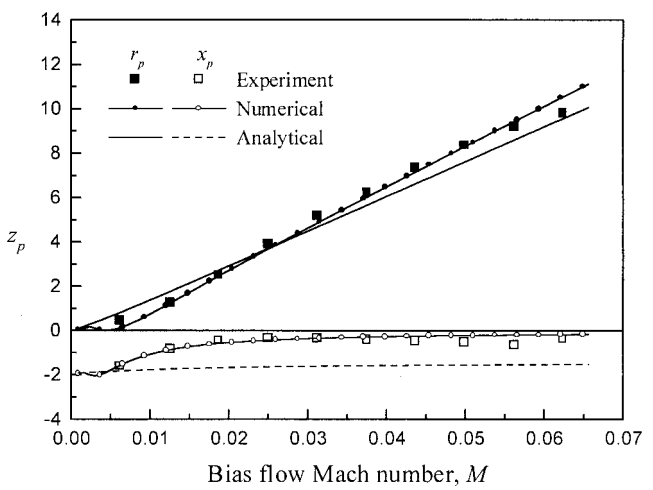

Fig. 7 Normalized acoustic impedance z_p plotted as a function of bias flow Mach number M for perforated plate 1; $T/R = 1.25$ and $kR = 8.87 \times 10^{-3}$.

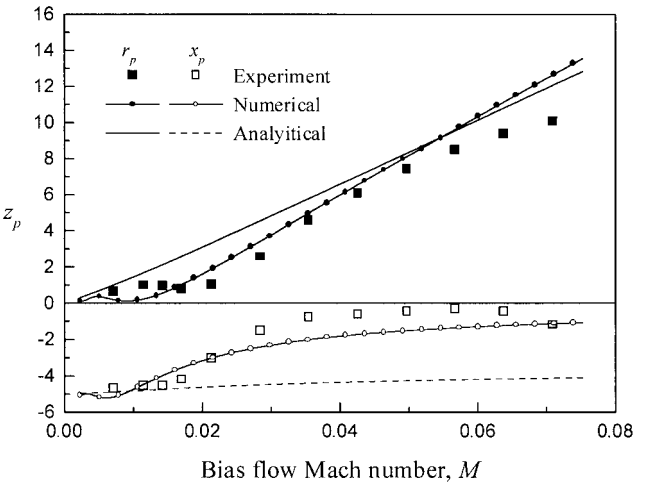

Fig. 8 Normalized acoustic impedance z_p plotted as a function of bias flow Mach number M for perforated plate 2; $T/R = 1.0$ and $kR = 2.22 \times 10^{-2}$.

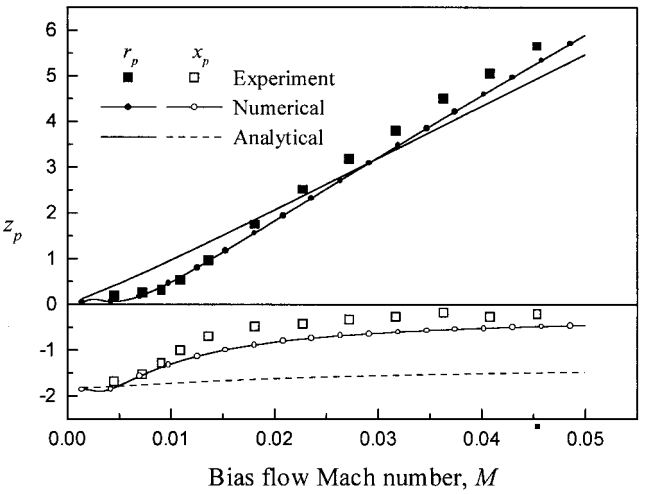

Fig. 9 Normalized acoustic impedance z_p plotted as a function of bias flow Mach number M for perforated plate 3; $T/R = 0.8$ and $kR = 1.39 \times 10^{-2}$.

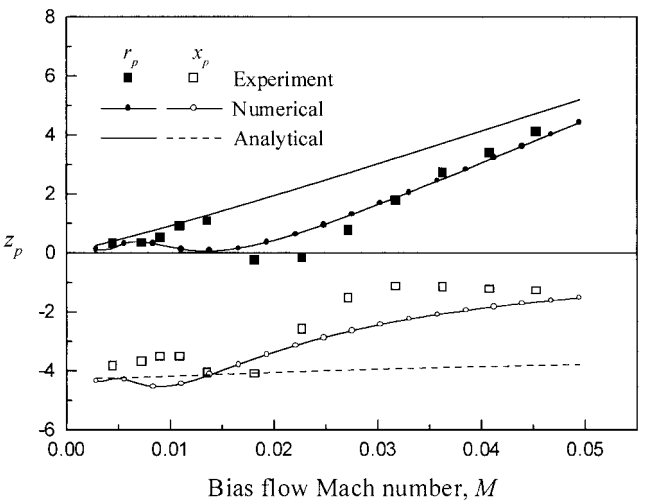

Fig. 10 Normalized acoustic impedance z_p plotted as a function of bias flow Mach number M for perforated plate 4; $T/R = 1.2$ and $kR = 2.77 \times 10^{-2}$.

flow. When the bias flow Mach number is near zero, the normalized specific acoustic reactance is approaching the classical value $-k(1.7R + T)/\sigma$. This result is expected because the effect of the bias flow gradually diminishes as the bias flow speed tends to zero. When the bias flow speed is increasing, the absolute value of the normalized specific acoustic reactance decreases. As a result, it loses all of the value due to the plate thickness at high bias flow speed. We try to give an explanation to this phenomenon. When the bias flow speed is high, the wavelength of the shed vortex wave is far larger than the orifice radius, and so the flow in the region downstream from the orifice inlet is in a quasi-steady state. In such a state the flow is almost quiescent outside the jet, so that the effect of the tube wall is expected to be little. In Figs. 7–10, it is also shown that plate thickness has a marked influence on the normalized specific acoustic resistance. As the bias flow speed increases, the increasing tendency of the normalized specific acoustic resistance is generally unchanged. However, within a certain range of the bias flow speed that is near to zero, the normalized specific acoustic resistance decreases with the increasing bias flow speed. By contrast, the normalized specific acoustic resistance linearly increases with the increase of the bias flow speed in the case of a thin plate. Kooi et al.[13] observed the decrease of the acoustic resistance of a thick perforated plate due to bias flow. However, no theoretical explanation is given in Ref. 13. Furthermore, the present numerical results show that, when $T/R > 1.5$, there exists a certain range of Strouhal number where δ is negative. Therefore, in this range of Strouhal numbers, the normalized specific acoustic resistance can even decrease to negative values according to Eq. (21). However, the normalized specific acoustic resistance is always positive for a thin perforated plate with bias flow. Both the present experimental and numerical results show that the effect of plate thickness on the acoustic resistance and acoustic reactance gradually diminishes at high flow speed. As a result, the acoustic properties of a thick perforated plate are similar to the corresponding thin one at high bias flow Mach number.

Note that the separated bias flow reattaches to the tube wall of an orifice when nondimensional plate thickness is large. When the reattachment happens, it is necessary to develop a model that takes such a factor into consideration to give good predictions of experiments.

VI. Conclusions

Acoustic properties in the presence of steady bias flow of a kind of perforated plate, which is constructed with square-edged orifices in a plate of small, but finite thickness, are studied. It is shown that plate thickness, which is characteristic of the real structure, has marked influence on both the acoustic resistance and the acoustic reactance.

1) When the bias flow speed is near zero, the acoustic reactance approaches the sum of the values due to the plate thickness and the end correction. As the flow speed increases, the acoustic reactance decreases. As a result, all of the value due to the plate thickness is lost at high flow speed.

2) As the bias flow speed increases, the increasing tendency of the acoustic resistance is generally unchanged. However, within a certain range of the bias flow speed that is near to zero, the acoustic resistance decreases with the increase of the bias flow speed. Furthermore, the present numerical results show that the acoustic resistance can even decrease to negative values provided that the ratio between the plate thickness and the orifice radius is larger than 1.5.

3) At high flow speed, the effect of plate thickness on the acoustic resistance and acoustic reactance gradually diminishes. Therefore, the acoustic properties of a thick perforated plate with bias flow are similar to the corresponding thin one.

4) The separation of the mean stream at the inlet edge of the orifice accounts for the described acoustic properties of a perforated plate with bias flow, which are by no means explained by the simple combination of the values due to the plate thickness with the end correction.

References

[1]Howe, M. S., "On the Theory of Unsteady High Reynolds Number Flow Through a Circular Aperture," *Proceedings of the Royal Society of London, Series A: Mathematics and Physical Sciences*, Vol. 366, 1979, pp. 205–223.

[2]Bechert, D. W., "Sound Absorption Caused by Vorticity Shedding, Demonstrated with a Jet Flow," *Journal of Sound and Vibration*, Vol. 70, No. 3, 1980, pp. 389–405.

[3]Hughes, I. J., and Dowling, A. P., "The Absorption of Sound by Perforated Linings," *Journal of Fluid Mechanics*, Vol. 218, 1990, pp. 299–335.

[4]Dean, P. D., and Tester, B. J., "Duct Wall Impedance Control as an Advanced Concept for Acoustic Suppresion," NASA CR-134998, 1975.

[5]Zhao, H., and Sun, X., "Active Control of Wall Acoustic Impedance," *AIAA Journal*, Vol. 37, No. 7, 1999, pp. 825–831.

[6]Sun, X., and Kaji, S., "Control of Blade Flutter by Use of Casing with Acoustic Treatment," Aeroengine Lab., Dept. of Aeronautics and Astronautics, Research Rept. 97-11, Univ. of Tokyo, Tokyo, 1998.

[7]Sun, X., and Kaji, S., "Effects of Wall Admittance Changes on Aeroelastic Stability of Turbomachines," *AIAA Journal* (to be published).

[8]Howe, M. S., "Influence of Wall Thickness on Rayleigh Conductivity and Flow-induced Aperture Tones," *Journal Fluids and Structures*, Vol. 11, 1997, pp. 351–366.

[9]Tan, L., "Numerical and Experimental Study on the Application of Perforated Plates with Bias Flow in Controlling the Sound Propagation in Ducts," M.S. Thesis, Dept. of Jet Propulsion, Beijing Univ. of Aeronautics and Astronautics, Beijing, March 1996.

[10]Rouse, H., and Abul-Fetouh, A., "Characteristics of Irrotational Flow through Axially Symmetric Orifices," *Journal of Applied Mechanics*, Vol. 17, No. 4, 1950, pp. 421–426.

[11]Struck, H. G., "Discontinuous Flows and Free Stream Line Solutions for Axisymmetric Bodies at Zero and Small Angles of Attack," NASA TN D-5634, 1970.

[12]Johnston, J. P., and Schmidt, W. E., "Measurement of Acoustic Reflection from an Obstruction in a Pipe with Flow," *Journal of the Acoustical Society of America*, Vol. 63, No. 5, 1978, pp. 1455–1460.

[13]Kooi, J. W., Sarin, S. L., and Fokker, B. V., "An Experimental Study of the Acoustic Impedance of Helmholtz Resonator Arrays Under a Turbulent Boundary Layer," AIAA Paper 81-1998, Oct. 1981.

P. J. Morris
Associate Editor